Insights into the Role of Na⁺ on the Transformation of Gypsum into α-Hemihydrate Whiskers in Alcohol−Water Systems

Hailu Fu,* Mengfan Li, Jianshi Huang, Shuang Cao, Jilei Lin, Mengxuan Yuan, and Guangming Jiang*

ACCESS | Metrics & More | Article Recommendations | Supporting Information

ABSTRACT: Alcohol−water solution-mediated transformation of gypsum into α-hemihydrate (α-HH) whiskers provides a green alternative for the high-value-added recycling of flue gas desulfurization (FGD) gypsum. However, the role of non-lattice cations during the transformation is still unclear. We report an evolution from "boosting−retarding" to "boosting−retarding−boosting" and finally to "boosting only" effect of non-lattice Na⁺ functioned by the concentration of ethylene glycol (EG) in water solutions. The driving force increased almost linearly upon the introduction of Na⁺ through the formation of ion pairs, and a higher slope was obtained at a higher EG concentration. Adsorption of Na⁺ ions and solidification of eugsterite on gypsum surfaces blocked the nucleation sites of α-HH. The retarding effect first rapidly increased and gradually approached a limit, following a parabolic trend after Na⁺ ions were introduced. Pentasalt, with a structure similar to that of α-HH, precipitated on the gypsum surface at higher $c(Na^+)$. The interaction of the driving force and the structural evolution of calcium sulfate ionic clusters accounts for the evolution of transformation kinetics. The retardation zone was compressed with the increase in EG volume ratios, and a monotonic boosting effect upon Na⁺ was observed at a 35.0 vol % of EG. Nucleation kinetics dominates the aspect ratio of α-HH whiskers. This study may provide a significant guidance for the utilization of FGD gypsum.
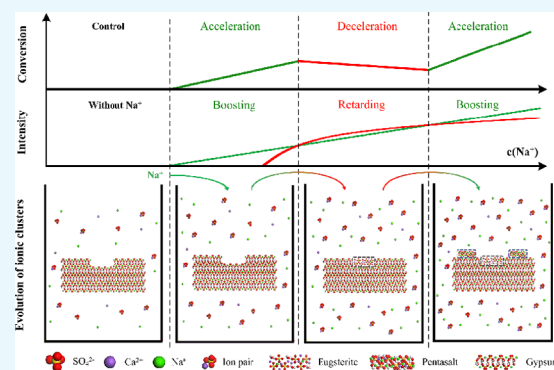
INTRODUCTION

Wet flue gas desulfurization (FGD) has proven to be an efficient sulfur dioxide (SO_2) emission control method. However, approximately 70−80 million tons of byproduct FGD gypsum is produced annually in China, which demands urgent recycling for the prevention of secondary pollution as well as for the conservation of the natural gypsum minerals.[1,2] Traditionally, FGD gypsum was utilized as a road sub-base, cement additive, plaster, or soil ameliorant.[3−6] Compared to these traditional ways, the synthesis of α-hemihydrate (α-HH) whiskers from the FGD gypsum precursor is a high-value-added alternative because of the excellent physicochemical properties of α-HH whiskers and promising applications in reinforcing agents, water treatment, water-in-oil emulsion purification, and so forth.[7−10]

Transformation of FGD gypsum to α-HH whiskers is preferentially performed using an autoclave-free method, considering operational safety and flexibility.[11,12] Alcohol−water systems are considered to be green conversion media compared to acid and chlorine−salt systems.[13−18] Water activity is considered to be an important thermodynamic factor that determines the phase transition direction and selective synthesis of calcium sulfate polymorphs.[19−21] Hydrogen bonds in alcohol−water solutions reduce the water activity, thus providing thermodynamic conditions that are favorable for the transformation. However, it is difficult for the conversion to occur in pure alcohol−water solutions.

The transformation process, which follows a dissolution−crystallization mechanism, is dominated by α-HH nucleation.[22,23] Moreover, nanorods of α-HH precipitate from calcium sulfate clusters, followed by orientational self-assembly to form bulk crystals.[24,25] The introduction of non-lattice cations significantly increases the concentration of ionic clusters through the formation of ion pairs between the nonlattice cations and sulfate.[26] Several studies have reported that the non-lattice cations significantly enhance the driving force and boost the conversion.[11,16,26,27] Owing to a relatively low interfacial energy, α-HH prefers to nucleate on the surface defects of gypsum.[28,29] However, inorganic cations may inhibit the calcium sulfate nucleation by adsorption or incorporation onto the crystal surface, blocking the nucleation sites.[30,31] Our previous study reported a "boosting−retarding" effect of Na⁺ ions in a 25.0 vol % ethylene glycol (EG)−water solution.[14]
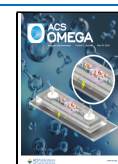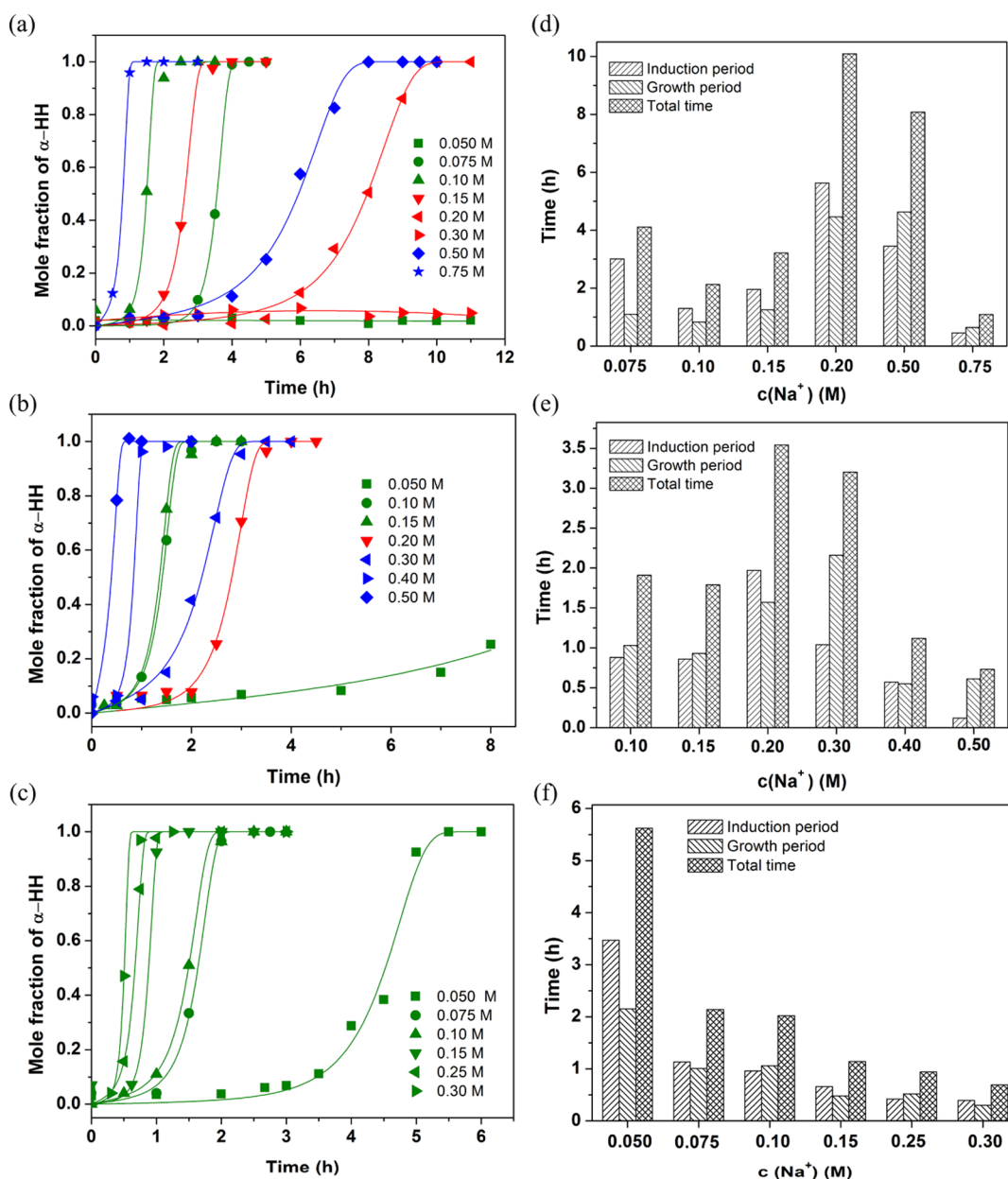
Figure 1. Effect of Na$^+$ on the transformation kinetics of gypsum to α-HH whiskers in EG−water solutions [(a,d) 25.0 vol %; (b,e) 30.0 vol %; and (c,f) 35.0 vol %] at 95.0 °C (note: the data in Figure 1a within 0.050−0.30 M Na$^+$ come from our previous published work[14]).

Doping of Na$^+$ ions on the gypsum surface by the formation of a solid solution of eugsterite blocks the nucleation sites of α-HH and retards the conversion. The underlying role of the non-lattice cations in the competition between the boosting and retarding effects is still not clear and requires further investigation.

When used as reinforcers, the mechanical properties of composites, such as rubbers, plastics, and ceramics, are closely related to the aspect ratio of the α-HH whiskers. Substantial effort has been devoted to control the morphologies of the α-HH whiskers.[12,17,32] Relative nucleation and growth rates among different crystal facets determine the final morphology of whiskers in nature. A rapid nucleation rate usually aggravates the agglomeration of α-HH whiskers via nucleus bridging, leading to a lower aspect ratio.[14,33] Certain additives are valid crystal modifiers, which include cations, such as Na$^+$, NH$_4^+$, Cu^{2+}, and Mg^{2+},[12,17,34,35] and cationic surfactants, such as

cetyltrimetyl ammonium bromide.[11] Preferential adsorption on the side facets of the α-HH whiskers facilitates one-dimensional (1-D) growth along the c-axis.[12] Furthermore, the morphology evolution of the α-HH whiskers depends on both the transformation kinetics and the modifiers.

In this study, we synthesized α-HH whiskers from a gypsum precursor in EG−water solutions to probe the effects of Na$^+$ ions on the transformation kinetics and the morphology evolution of the α-HH whiskers. We first report a "boosting− retarding−boosting" effect of the Na$^+$ ions on the gypsum−α-HH whiskers conversion. The competition between the boosting and retarding effects of the Na$^+$ ions is revealed from the driving force and steric hindrance of nucleation. Finally, the adsorption of Na$^+$ ions and structural evolution of the ion pairs in various EG−water solutions are systematically analyzed.

■ EXPERIMENTAL SECTION

Materials. Chemical regents including EG ($C_2H_6O_2$, purity ≥ 99.0%), calcium sulfate dihydrate (DH; $CaSO_4·2H_2O$, purity ≥ 99.0%), and sodium chloride (NaCl, purity ≥ 99.5%) were of analytical grade and purchased from Sinopharm Chemical Reagent Co., Ltd. China. Deionized water was used in all experiments.

Preparation of α-HH Whiskers in EG−Water Solutions. The conversion media containing 25.0−35.0 vol % EG and 0−1.0 M Na^+ ions were prepared by mixing EG and sodium chloride in deionized water. Then, the stock solution was transferred into a 1 L glass-jacketed reactor, stirred with a 250 rpm Teflon impeller, and heated by circulating oil in the jacket. The temperature of the stock solution was monitored with a thermometer. Conversion of gypsum (initial solid content of 5.0 wt %) to α-HH whiskers was carried out at 95.0 °C and atmospheric pressure. Hot suspensions were withdrawn and treated with vacuum filtration in a funnel. The solids were collected after being rinsed with hot water and ethanol sequentially and dried in an oven at 45.0 °C. The conversion progress was tracked by solid characterizations. Hot suspensions also were micro-filtered with a 0.22 μm membrane, and the sulfate concentration in the filtrate were determined according to the turbidity method using PC MultiDirect COD Vario Moving Labs (ET99731, Tintometer GmbH Germany)[28] To explore the Na^+ adsorption/doping, suspensions were collected at different time intervals and treated with vacuum filtration only before drying at 45.0 °C. The contents of Na^+ in the solids were determined by dissolving the solids into the 2 wt % nitric acid solution and measuring the Na^+ concentrations using a inductively coupled plasma−optical emission spectrometer (Agilent 5100, USA).

Solid Characterization. Crystal water contents of the solids were determined by the mass loss during calcination at 350.0 °C using thermogravimetry and differential scanning calorimetry (STA-409PC, NET-ZSCH, Germany). The mole fraction evolution during gypsum−α-HH transformation was calculated based on the crystal water content. The morphology was examined by scanning electron microscopy (HITACHIS-4800 Japan), and the aspect ratio (L/W) was determined by measuring the lengths and widths of approximate 200 α-HH whiskers using the equipped software. X-ray diffraction (XRD, D/Max-2500pc, Rigaku, Inc.) analysis was performed with Cu Kα radiation with a resolution of 0.02° in the 2θ range of 10−80° to further determine the solid structure. The solid surfaces were characterized by X-ray photoelectron spectroscopy (XPS, ESCALAB 250Xi, Thermo Fisher Scientific, USA) with Al Kα energy of 1486.6 eV to determine the presence of Na^+ ions and their association with the solid surfaces or the crystal structures. High-resolution transmission electron microscopy (HR-TEM; FEI-Tecnai G2, USA) and selected area electron diffraction were performed at an accelerating voltage of 300 kV to identify the surface precipitation of solid solutions.

■ RESULTS AND DISCUSSION

Effects of Na^+ Ions on the Transformation Kinetics of Gypsum−α-HH Whiskers. The effect of Na^+ on the conversion kinetics in 25.0, 30.0, and 35.0 vol % EG−water solutions is shown in Figure 1. The hemihydrate whisker is of α-type (α-HH) characterized by DSC analysis (detailed information refers to the Supporting Information). Our previous study[14] showed a "boosting−retarding" effect upon

$c(Na^+)$ during gypsum−α-HH conversion in 25.0 vol % EG−water solutions. The conversion ceased completely when $c(Na^+)$ was 0.30 M. However, in 30.0 vol % EG solutions, when the $c(Na^+)$ are within 0.050−0.15, 0.15−0.20, and 0.20−0.50 M, the conversion accelerates, decelerates, and accelerates again, respectively. The "boosting−retarding−boosting" effect of the non-lattice Na^+ on the calcium sulfate phase transition was first reported in alcohol−water systems. When we further increased $c(Na^+)$ to 0.75 M in 25.0 vol % EG−water solutions, the conversion surprisingly resumed and accelerated with a higher $c(Na^+)$ (Figure 1). Upon increasing $c(Na^+)$, the retarding zone in the 30.0 vol % EG−water systems was compressed when compared with that in 25.0 vol % solutions. The retarding zone in the 35.0 vol % EG−water system disappeared, and the conversion monotonically accelerated with the increase in $c(Na^+)$. The monotonous boosting effect within 0−0.30 M Na^+ in 35.0 vol % EG−water solutions was consistent with most published results.[11,16,26,27]

To further investigate the transformation kinetics, we divided the transformation process into two stages at the 10 mol % conversion point,[29,36] before and after which the stages represent the induction and growth periods for α-HH crystallization, respectively. The boosting or retarding effect mainly depends on the nucleation process of α-HH. The induction period (t_{ind}) for 0.075−0.20 M Na^+ in the 25.0 vol % EG−water system was longer than the growth period, indicating that the transformation is a nucleation-controlled process. However, the induction period at 0.50 and 0.75 M Na^+ was shorter than the growth period, which implies that the growth of α-HH dominates the conversion. Solution-mediated calcium sulfate phase transformation is a dissolution−nucleation process, and its induction period is usually longer than the growth period.[37] When several nucleation sites occupy the mother crystal surface, steric hindrance may prolong the growth time.[29] The dominant step shifts from nucleation to growth as a function of $c(Na^+)$. A similar phenomenon was also observed in the 30.0 vol % EG−water systems. Nucleation of α-HH continues to be the controlling step within the studied $c(Na^+)$ scope in 35.0 vol % EG−water solutions, which indicates that the boosting effect from nucleation nullifies the steric hindrance effect.

Figure 2 shows the effect of Na^+ on the nucleation rate (defined as $1/t_{ind}$) at different EG concentrations. In 25.0 vol % EG−water solutions, the nucleation rate increased until $c(Na^+)$ reached 0.10 M, then decreased from 0.10 to 0.30 M, and finally increased again at $c(Na^+)$ 0.30−0.75 M. The nucleation rate in 30.0 vol % EG−water solutions evolved with the same trend as that observed in 25.0 vol % EG−water solutions. The difference lies in the fact that the retardation effect of Na^+ was reduced for $c(Na^+)$ between 0.15 and 0.20 M, and the nucleation rate did not drop to zero at the strongest retardation point. A monotonic boosting effect of Na^+ on the nucleation rate was observed in 35.0 vol % EG solutions. The retarding effect of Na^+ tends to be alleviated, and α-HH nucleation tends to achieve a higher rate in higher EG volume ratio solutions within 0.05−0.30 M Na^+.

Concentration and Structural Evolution of Sulfate Ionic Clusters. The $c(SO_4^{2-})$ was tested to evaluate the effect of Na^+ on the driving force evolution. Generally, the solubility of DH increased upon Na^+ in all EG−water solutions due to the formation of sodium-sulfate ion pairs ($[Na_2SO_4]^0$), which increases the driving force of transformation. The solubility of DH decreased with the increase in EG volume ratio at the
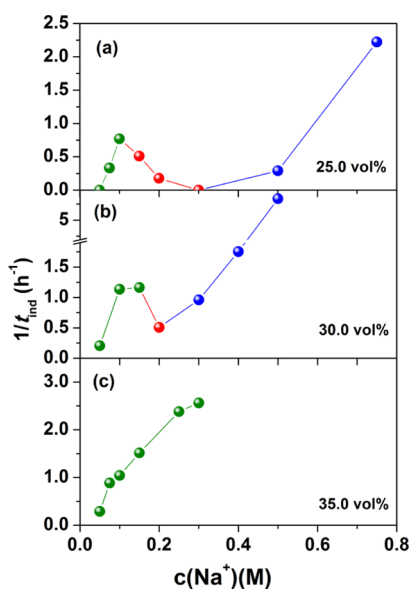
Figure 2. Effect of Na^+ on the nucleation rate $(1/t_{ind})$ of α-HH in different EG−water solutions [(a) 25.0 vol %; (b) 30.0 vol %; and (c) 35.0 vol %].

same $c(Na^+)$. This is attributed to the lower water activity in concentrated EG−water solutions, which resembles the solubility of gypsum in salt solutions.[37] The solubility of DH in the EG solutions increased almost linearly with the increase in $c(Na^+)$ (Figure 3). The slope (Table 1) increases from
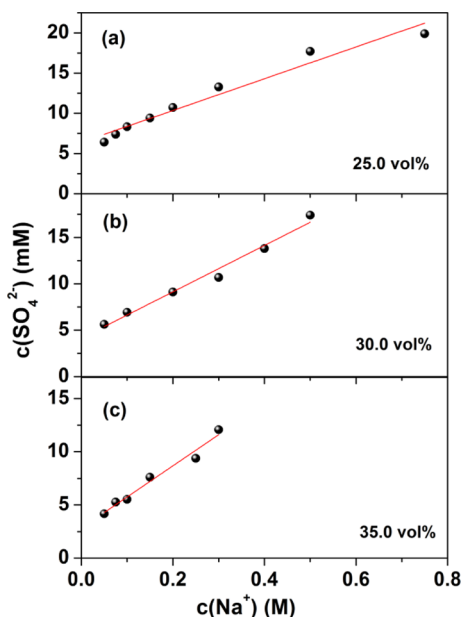

Figure 3. Effect of Na^+ on the DH solubility in different EG−water solutions. [(a) 25.0 vol %; (b) 30.0 vol %; (c) 35.0 vol %].

Table 1. DH's Solubility Evolution Slopes Upon Na^+ in Different EG−Water Solutions

volume fraction	slopes (mM SO_4^{2-}/M Na^+)	relationship
25.0 vol %	19.78	$y = 19.78x + 6.40$
30.0 vol %	25.01	$y = 25.01x + 4.13$
35.0 vol %	29.27	$y = 29.27x + 2.82$

19.78 to 29.27 mM $c(SO_4^{2-})$/M $c(Na^+)$, which indicates that Na^+ induces a larger driving force variation within the same $c(Na^+)$ change. We therefore deduce that a larger boosting effect of Na^+ is produced with higher EG volume ratios.

Our previous study[14] showed that the precipitation of eugsterite $[Na_4Ca(SO_4)_3 \cdot 2H_2O$, JCPDS 35-0487] on the DH crystal surface blocked the nucleation sites of α-HH and retarded the transformation from DH to α-HH. We assume that solidification of ion-pair clusters into eugsterite may attain equilibrium owing to limited surface defects of gypsum. The adsorption capacity of Na^+ onto the gypsum surface was investigated in 25.0 vol % EG−water solutions at 70.0 °C in order to avoid phase transformation. The results showed that the adsorption of Na^+ on the DH surface rapidly attained equilibrium within 1.0 h (Figure 4), and no further adsorption
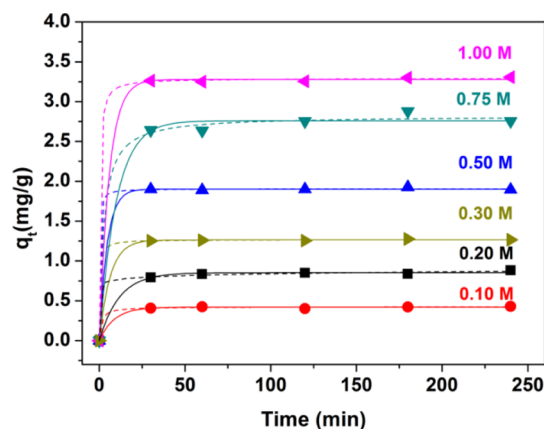

Figure 4. Na^+ adsorption kinetics of DH in 25.0 vol % EG−water solutions at 70.0 °C("−" simulated by the PFO model; "---" simulated by the PSO kinetic model).

occurred in the subsequent 3 h. The adsorption kinetics were simulated using pseudo-first-order (PFO) and pseudo-second-order (PSO) kinetic models (eqs 1 and 2, respectively).[38,39]

$$q_t = q_e(1 - \exp(-k_1 t)) \tag{1}$$

$$q_t = (k_2(q_e)^2 t)/(1 + k_2 q_e t) \tag{2}$$

where q_t (mg/g) and q_e (mg/g) are the amounts of Na^+ adsorbed at time t and at equilibrium, respectively, and k_1 (min^{-1}) and k_2 (g/mg min) are the PFO and PSO rate constants, respectively. The adsorption of Na^+ on DH can be better simulated by the PFO model, as the experimental equilibrium adsorption capacity (q_e) values are quite close to those calculated from the PFO model, as listed in Table 2. For example, the experimental q_e value at 0.20 M Na^+ is 0.8509 mg/g DH, while the calculated values from the PFO and PSO models are 0.8525 and 0.8396 mg/g DH, respectively. It can be inferred that the adsorption kinetics are mainly controlled by diffusion rather than the surface combination of Na^+.[40,41]

We also obtained the adsorption isotherms using the Langmuir and Freundlich adsorption models using the following equations (eqs 3 and 4).[42,43]

$$q_e = q_m(k_L C_e)/(1 + k_L C_e) \tag{3}$$

$$q_e = k_F(C_e)^{1/n} \tag{4}$$

Table 2. Kinetic Parameters of Na$^+$ Adsorption onto Gypum in 25.0 vol % EG−Water Solutions at 70.0 °C

	PFO model			PSO model		
$c(Na^+)$ (M)	k_1 (min^{-1-1})	q_e (mg/g)	R^2	$k_2 \times 10^3$ (g/mg·min^{-1})	q_e (mg/g)	R^2
0.10	0.1167	0.4197	0.9964	2.0868	0.3235	0.9963
0.20	0.08725	0.8525	0.9971	2.0626	0.8396	0.9910
0.30	0.1609	1.2642	0.9998	2.0993	1.2686	0.9998
0.50	0.2215	1.9025	0.9997	2.8572	1.9067	0.9997
0.75	0.1018	2.7597	0.9943	0.1445	2.9219	0.9965
1.00	0.1761	3.2784	0.9996	0.7723	3.2925	0.9997

where q_e (mg/g) and C_e (mg/L) are the equilibrium adsorption capacity and equilibrium concentration of Na$^+$ in solution, respectively; k_L (L/mg) is the constant related to the number of surface sites per unit mass of the adsorbent; q_m (mg/g) is the maximum value of Na$^+$ adsorption per unit mass of the adsorbent; and k_F (mg/g·(L/mg)$^{1/n}$) and n are Freundlich parameters related to the adsorption capacity and adsorption intensity. The results (Figure 5 and Table 3) show
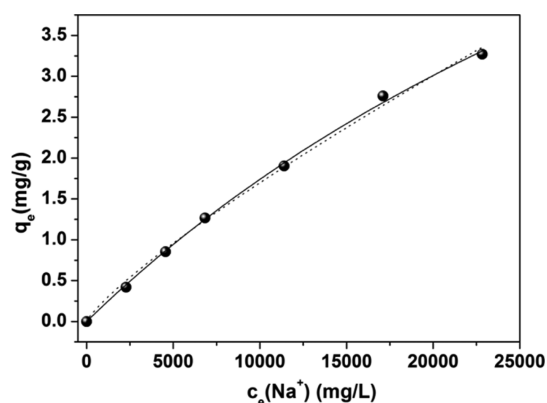

Figure 5. Adsorption isotherms of Na$^+$ onto DH in 25.0 vol % EG−water solutions at 70.0 °C ("−" simulated by the Langmuir model; "⋯⋯" simulated by the Freundlich model).

that the adsorption of Na$^+$ onto DH better fits the Langmuir model, and the maximum adsorption capacity (q_{max}) is 11.16 mg/g DH. It can be inferred that the monolayer adsorption of Na$^+$ tends to occur on a flat DH crystal surface with a relatively uniform distribution of the energetic adsorption sites, which is consistent with the published results of the adsorption of Pb^{2+} using HH.[44] Herein, the adsorption results indicate that the adsorption of Na$^+$ onto DH may achieve equilibrium during the gypsum−α-HH conversion.

The elemental concentration of adsorbed Na$^+$ was analyzed by XPS. In Figure 6, Na$^+$ is hardly detectable in the control sample (raw gypsum). The peak intensity gradually increases between 0.10 and 0.30 M and changed little between 0.30 and 1.00 M. The relative elemental concentration of surface Na$^+$ (Table 4) increased from 0.14 to 0.45 at. % when $c(Na^+)$ increased from 0 to 0.30 M and fluctuated slightly within 0.40−0.45 at. % when $c(Na^+)$ further increased to 1.00 M. The Ca/S ratio decreased from 0.9230 to 0.8936 between 0 and
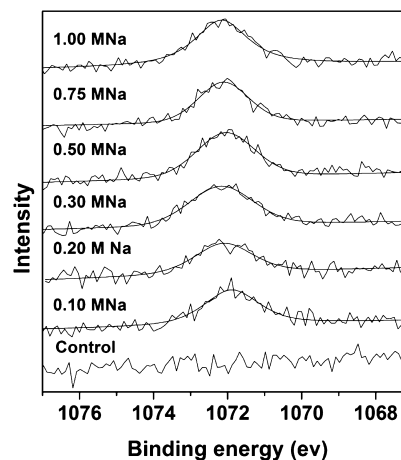

Figure 6. XPS patterns of DHs influenced by Na$^+$ in 25.0 vol % EG−water solutions at 70.0 °C.

0.30 M Na$^+$ and then slightly increased to 0.9034−0.9073 as $c(Na^+)$ further increased to 1.00 M (Figure 7). The surface Na$^+$ reached the saturation point at 0.30 M and no more Na$^+$ adsorption occurred above 0.30 M. This may account for the limited retarding effect in a wide range of $c(Na^+)$.

The solid components were characterized by the XRD patterns. Apart from the characteristic peaks of DH at $2\theta =$ 31.080, 32.058, 33.338, 34.480, 40.601, and 47.818° (JCPDS 33-0311), the peaks at $2\theta = 39.296$ and 46.402° indicate the existence of eugsterite [Na$_4$Ca(SO$_4$)$_3$·2H$_2$O, JCPDS 35-0487] (Figure 8a). Based on our previous study,[14] the formation of eugsterite blocked the nucleation sites of α-HH, resulting in the retardation effect of the Na$^+$ ions. It should be noted that the peak intensity did not increase significantly with the increase in $c(Na^+)$, suggesting that the retarding effect of eugsterite on the nucleation rate reached a limit at a certain threshold $c(Na^+)$ value. Pentasalt [Na$_2$Ca$_5$(SO$_4$)$_6$·3H$_2$O, JCPDS 41-0224], characterized by the peak at $2\theta = 31.672°$ was observed in the solids obtained with a $c(Na^+)$ higher than 0.50 M (Figure 8b). The peak intensity increased with the increase in $c(Na^+)$, which indicates that more pentasalt precipitated from the solution. As the Ca/S ratios of eugsterite and pentasalt are 1:3 and 5:6, respectively, more precipitation of pentasalt led to a relatively higher surface Ca/S ratio at higher $c(Na^+)$ (i.e., 0.50−1.0 M), as shown in Figure 7. The

Table 3. Isotherm Parameters of the Adsorption of Na$^+$ onto the DH Surfaces

	Langmuir model			Freundlich model		
k_L (L/mg)	q_m (mg/g)	R^2	k_F mg/g·(L/mg)$^{1/n}$	$1/n$	R^2	
1.847×10^{-5}	11.16	0.9985	8.42×10^{-4}	0.8261	0.9960	

Table 4. Elemental Composition in DH Surfaces Detected by XPS

$c(Na^+)$ (M)	0	0.10	0.20	0.30	0.50	0.75	1.00
Na (at. %)	0.14	0.26	0.18	0.45	0.4	0.45	0.43
O (at. %)	60.1	58.68	55.65	56.48	56.15	58.15	57.47
S (at. %)	14.16	13.66	13.57	13.72	13.57	13.99	13.81
Ca (at. %)	13.07	12.53	12.21	12.26	12.26	12.65	12.53
C (at. %) (background)	12.52	14.86	18.39	17.09	17.61	14.76	15.77
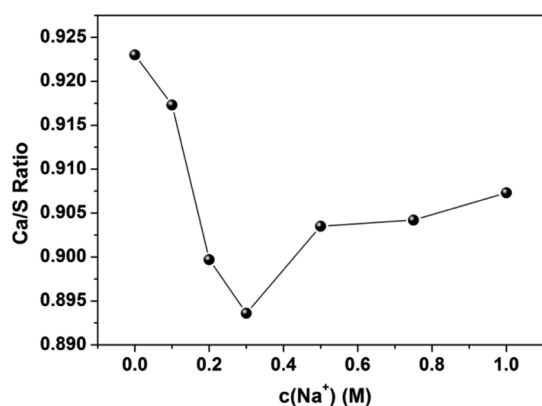
Figure 7. Effect of Na^+ on the Ca/S ratio of the DHs.

Figure 9. HR-TEM images of the solid solutions formed on the gypsum surface [(a,b) eugsterite; (c,d) pentasalt].

precipitation of pentasalt may boost the nucleation of α-HH as both compounds share similar structures.

The formation of solid solutions (i.e., eugsterite and pentasalt) on gypsum surface was further characterized by HR-TEM. A square plate-like solid was formed (Figure 9a) at the corner of the surface of the mother DH crystals owing to the low interfacial energy. The spot pattern (inset) demonstrated a perfect single crystal structure. Interplanar spacings of 3.424, 3.065, 4.551, and 4.634 Å indicated that the solid was probably composed of eugsterite. The lattice fringe spacings (Figure 9b) of 2.662 and 2.679 Å characterize the crystal plane at $2\theta = 33.523°$, and the spacing of 2.309 Å characterizes the crystal plane at $2\theta = 39.293°$. These observations are consistent with the XRD peaks of eugsterite observed in Figure 8a. Fine needle-like solid particles were observed on the gypsum surface in Figure 9c, and the spot pattern (inset) demonstrates a well-developed single crystal. The interplanar spacings of 6.081 and 2.237 Å indicated that the solid particles were probably composed of pentasalt. The lattice infringe spacings of 2.348 and 2.721 Å (Figure 9d)
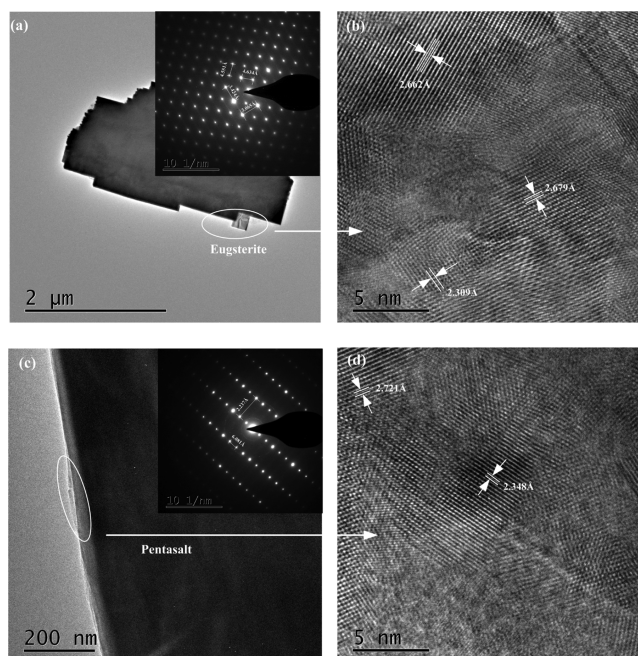
correspond to the crystal planes at $2\theta = 38.208$ and $31.676°$ (Figure 8b), respectively.

Illustration of the Retarding and Boosting Effects and Their Influence on the Morphologies of the α-HH Whiskers. We conclude that the driving force increases with the increase in $c(Na^+)$ owing to the formation of $[Na_2SO_4]^0$ ion pairs (Figure 10). The nucleation of α-HH was boosted from the point of increasing driving force. Adsorption of Na^+ ions on the gypsum surface and solidification of the ion pairs into the eugsterite lead to the blockage of the nucleation sites of the α-HH whiskers. The retarding effect probably reaches a limit at relatively lower $c(Na^+)$. Pentasalt begins to precipitate
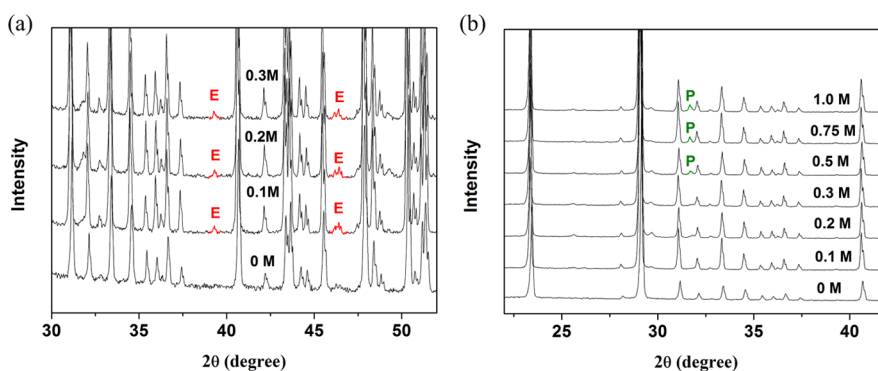

Figure 8. XRD patterns of solids obtained in 25.0 vol % EG−water solutions at 70.0 °C at different time intervals [(a) eugsterite (E); (b) pentasalt (P)].
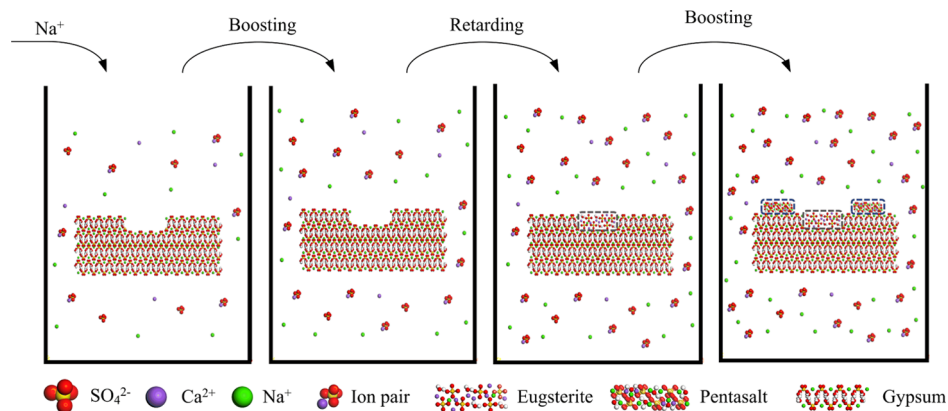
Figure 10. Schematic program of the "boosting−retarding−boosting" effect on DH−α-HH transformation along the $c(Na^+)$ in a 30.0 vol % EG−water solution.

Figure 11. Illustration on the effect of $c(Na^+)$ on the DH−α-HH conversion in different EG−water solutions.

Figure 12. Morphology evolution (a,b) and the relationship between the L/W of whiskers and nucleation rates ($1/t_{ind}$) [(c) 30.0 vol %, (d) 35.0 vol %].

from the solutions as $c(\text{Na}^+)$ exceeds a certain threshold, which favors α-HH nucleation from the view of similar structure an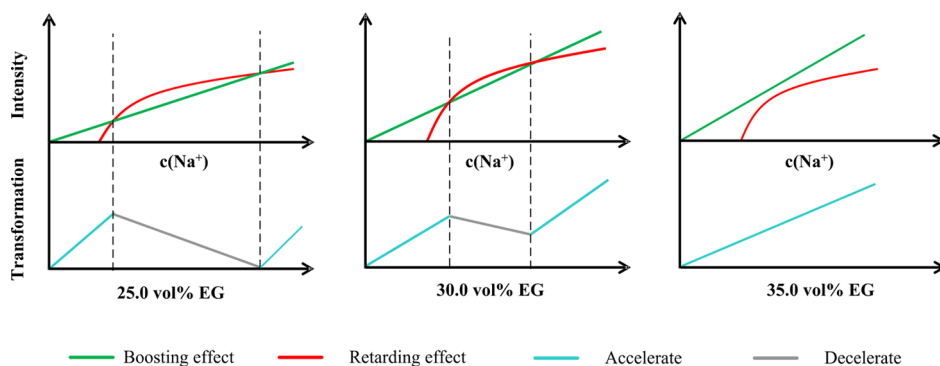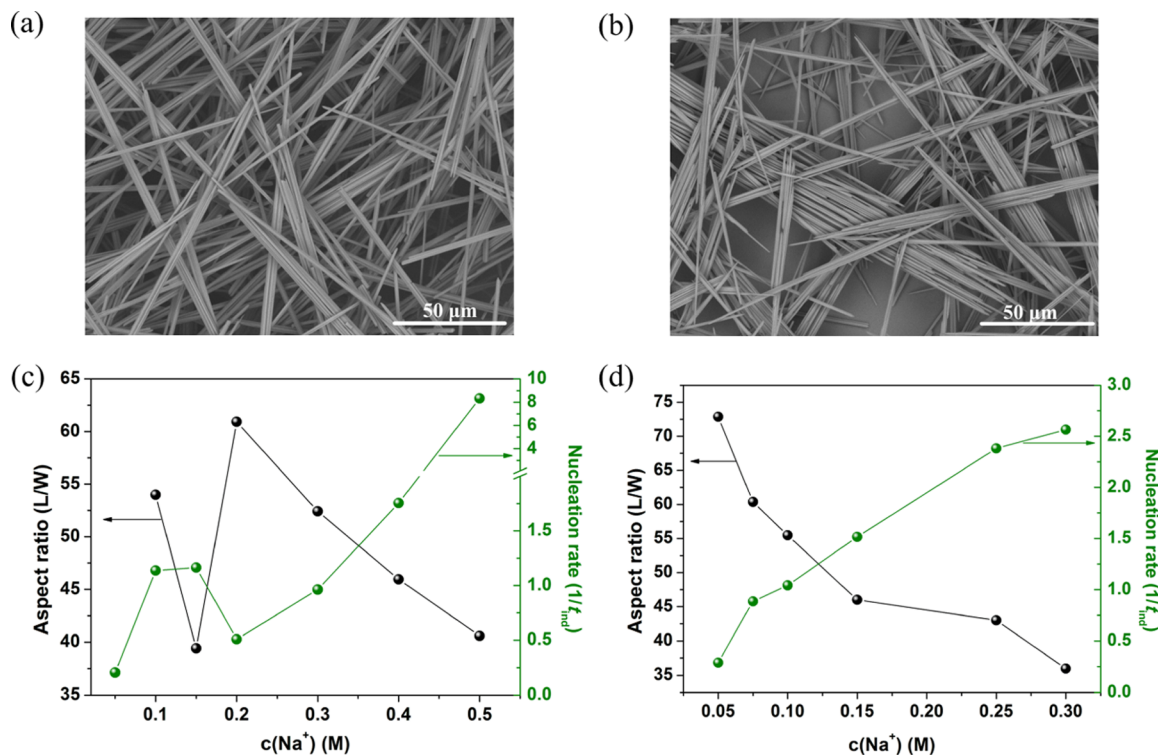d lower interfacial energy. Combined the stronger driving force and occurrence of pentasalt (acting as nuclei for α-HH nucleation), the conversion breaks through the retarding effect and accelerates again upon further increasing $c(\text{Na}^+)$.

The "boosting–retarding–boosting" effect depends on both the EG volume ratio and $c(\text{Na}^+)$ (Figure 11). When the EG volume ratio is low, the boosting effect originating from the ion pairs (higher driving force) is stronger than the retarding effect caused by eugsterite precipitation blockage of the nucleation sites at low $c(\text{Na}^+)$. However, with the increase in $c(\text{Na}^+)$, the retarding effect increases rapidly compared to the boosting effect, leading to an overall retarding effect. This accounts for the transformation in the 25.0 vol % EG–water solution influenced by the Na$^+$ ions within 0–0.30 M.[14] As the retarding effect reaches a maximum limit with the increase in $c(\text{Na}^+)$, the boosting effect from the increasing driving force and pentasalt counteracts the retarding effect, creating an overall rate accelerating effect, and the transformation reaccelerates with the increase in $c(\text{Na}^+)$. The increasing volume ratio of EG in the solutions shrinks the retardation zone owing to the rapidly increasing driving force (i.e., higher slope) and the formation of pentasalt. When the volume ratio of EG exceeds a certain limit, the retarding effect from eugsterite is completely inhibited, and the net effect is only the boosting effect from the Na$^+$ ions.

We also investigated the change in the α-HH whisker aspect ratio with the increase in $c(\text{Na}^+)$ in different EG–water solutions. Na$^+$ tends to adsorb onto the side facet of the α-HH whiskers, preferentially along the c-axis because of steric hindrance. 1-D morphology of α-HH is desired to obtain a higher aspect ratio with a smaller width (Figure 12a). Agglomeration of the whiskers increases the width and significantly reduces the aspect ratio (Figure 12b). Higher nucleation rate with the increase in $c(\text{Na}^+)$ results in insufficient development of crystals, whereas the aggregation of nuclei and interlock growth results in shuttle-shaped whiskers. Therefore, the coordinated effect of nucleus bridging on the introduction of Na$^+$ and nucleation rate determines the agglomeration degree of the whiskers in 25.0 vol % EG–water solution.[14] In the 30.0 and 35.0 vol % EG–water solutions (Figure 12c,d), the aspect ratio was inversely proportional to the nucleation rate. In the 35.0 vol % EG–water solution, the L/W ratio of the whiskers decreased from 72.86 to 35.95 with the increase in $c(\text{Na}^+)$. Therefore, a higher $c(\text{Na}^+)$ value did not produce higher L/W ratios. The length of the whiskers decreased significantly with the increase in width (detailed information provided in Table S1). Therefore, the transformation kinetics determines the final morphology to a relatively larger degree. We also tried the conversion of FGD gypsum into α-HH whiskers in EG–water solutions with the addition of Na$^+$. The results showed that FGD gypsum can be transformed into α-HH whiskers in a 40.0 vol % EG–water solution mixed with 0.10 M Na$^+$ at 95.0 °C (detailed information refers to the Supporting Information). Taking FGD gypsum characteristics into consideration, more effort is required to optimize the process for FGD gypsum utilization in the future.

CONCLUSIONS

Sodium cation-mediated transformation of gypsum–α-HH whiskers in EG–water solutions was investigated to study the transformation kinetics and morphology evolution. The introduction of a non-lattice Na$^+$ induced a "boosting–retarding–boosting" effect during calcium sulfate phase transition in alcohol–water systems. Elevation of the driving force and formation of pentasalt (acting as nuclei) formation account for the boosting effect, which strengthens linearly upon $c(\text{Na}^+)$ and with a steeper slope at higher EG volume fractions. The retarding effect caused by the surface adsorption on eugsterite and blockage of the nucleation sites increased rapidly at low $c(\text{Na}^+)$ values and then gradually reached a certain limit. The interaction between the boosting and retarding effects accounts for the evolution of the transformation rate. The driving force increased with the increase in EG volume ratio, whereas the retarding effect evolved in a similar way but to a lesser extent. Only the boosting effect on the introduction of Na$^+$ was observed in systems with a higher EG volume ratio. The transformation kinetics determined the aspect ratio to a large extent. The aspect ratio evolved in an inversely proportional manner with the nucleation rate. Obtaining 1-D whiskers with a high aspect ratio and a high transformation rate will be investigated in the future.

■ ASSOCIATED CONTENT

Ⓢ Supporting Information

The Supporting Information is available free of charge at https://pubs.acs.org/doi/10.1021/acsomega.2c00347.

> Characterization of the α-type hemihydrate, lengths and widths of the whiskers, and the transformation of FGD gypsum into α-HH whiskers (PDF)

■ AUTHOR INFORMATION

Corresponding Authors

Hailu Fu − *Department of Environmental Engineering, China Jiliang University, Hangzhou 310018, China;* ⓞ orcid.org/0000-0003-0726-4693; Phone: +86 571 87676357; Email: hlfu@cjlu.edu.cn; Fax: +86 571 8767226

Guangming Jiang − *Engineering Research Center for Waste Oil Recovery Technology and Equipment, Ministry of Education, Chongqing Technology and Business University, Chongqing 400067, China;* ⓞ orcid.org/0000-0002-7375-0107; Phone: +86 23 62769787; Email: jiangguangming@zju.edu.cn

Authors

Mengfan Li − *Department of Environmental Engineering, China Jiliang University, Hangzhou 310018, China*

Jianshi Huang − *Department of Environmental Engineering, China Jiliang University, Hangzhou 310018, China*

Shuang Cao − *Department of Environmental Engineering, China Jiliang University, Hangzhou 310018, China*

Jilei Lin − *Department of Environmental Engineering, China Jiliang University, Hangzhou 310018, China*

Mengxuan Yuan − *Department of Environmental Engineering, China Jiliang University, Hangzhou 310018, China*

Complete contact information is available at:
https://pubs.acs.org/10.1021/acsomega.2c00347

Notes

The authors declare no competing financial interest.

■ ACKNOWLEDGMENTS

■ REFERENCES

(1) Zhao, S.; Duan, Y.; Lu, J.; Gupta, R.; Pudasainee, D.; Liu, S.; Liu, M.; Lu, J. Thermal stability, chemical speciation and leaching characteristics of hazardous trace elements in FGD gypsum from coal-fired power plants. *Fuel* **2018**, *231*, 94−100.

(2) Liu, Z.; Hao, Y.; Zhang, J.; Wu, S.; Pan, Y.; Zhou, J.; Qian, G. The characteristics of arsenic in Chinese coal-fired power plant flue gas desulphurisation gypsum. *Fuel* **2020**, *271*, 117515.

(3) Hua, M.; Wang, B.; Chen, L.; Wang, Y.; Quynh, V. M.; He, B.; Li, X. Verification of lime and water glass stabilized FGD gypsum as road sub-base. *Fuel* **2010**, *89*, 1812−1817.

(4) Xu, L.; Wu, K.; Li, N.; Zhou, X.; Wang, P. Utilization of flue gas desulfurization gypsum for producing calcium sulfoaluminate cement. *J. Cleaner Prod.* **2017**, *161*, 803−811.

(5) Pedreño-Rojas, M. A.; Fort, J.; Cerny, R.; Rubio-de-Hita, P. Life cycle assessment of natural and recycled gypsum production in the Spanish context. *J. Cleaner Prod.* **2020**, *253*, 120056.

(6) Wang, J.; Yang, P. Potential flue gas desulfurization gypsum utilization in agriculture: A comprehensive review. *Renewable Sustainable Energy Rev.* **2018**, *82*, 1969−1978.

(7) Zhang, G.; Cao, D.; Wang, Y.; Guo, S.; Yang, Z.; Cui, P.; Wang, Q.; Dou, Y.; Cheng, S.; Shen, H. alpha-calcium sulfate hemihydrate with a 3D hierarchical straw-sheaf morphology for use as a remove Pb^{2+} adsorbent. *Chemosphere* **2022**, *287*, 132025.

(8) Wang, L.; Huang, Y.; Zhou, D.; Chen, X.; Zhao, H.; Li, X.; Hughes, S. S.; Zhang, P.; He, P.; Zhang, G.; Cheng, X.; Zhang, R. Efficient removal of fluoride from neutral wastewater by green synthesized Zr/calcium sulfate whiskers: An experimental and theoretical study. *Colloids Surf., A* **2021**, *630*, 127587.

(9) Jiang, G.; Fu, W.; Wang, Y.; Liu, X.; Zhang, Y.; Dong, F.; Zhang, Z.; Zhang, X.; Huang, Y.; Zhang, S.; Lv, X. Calcium sulfate hemihydrate nanowires: one robust material in separation of water from water-in-oil emulsion. *Environ. Sci. Technol.* **2017**, *51*, 10519−10525.

(10) Ma, F.; Chen, C.; Wang, Y. Mechanical behavior of calcium sulfate whisker-reinforced paraffin/gypsum composites. *Constr. Build. Mater.* **2021**, *305*, 124795.

(11) Guan, Q.; Sun, W.; Hu, Y.; Yin, Z.; Guan, C. A facile method of transforming FGD gypsum to alpha-$CaSO_4 \cdot 0.5H_2O$ whiskers with cetyltrimethylammonium bromide (CTAB) and KCl in glycerol-water solution. *Sci. Rep.* **2017**, *7*, 7085.

(12) Hou, S.; Wang, J.; Wang, X.; Chen, H.; Xiang, L. Effect of Mg^{2+} on hydrothermal formation of alpha-$CaSO_4 \cdot 0.5H_2O$ whiskers with high aspect ratios. *Langmuir* **2014**, *30*, 9804−9810.

(13) Guan, Q.; Hu, Y.; Tang, H.; Sun, W.; Gao, Z. Preparation of alpha-$CaSO_4 \cdot 1/2H_2O$ with tunable morphology from flue gas desulphurization gypsum using malic acid as modifier: A theoretical and experimental study. *J. Colloid Interface Sci.* **2018**, *530*, 292−301.

(14) Fu, H.; Huang, J.; Shen, L.; Li, Y.; Xu, L.; Wei, F.; Li, J.; Jiang, G. Sodium Cation-Mediated Crystallization of α-Hemihydrate Whiskers from Gypsum in Ethylene Glycol-Water Solutions. *Cryst. Growth Des.* **2018**, *18*, 6694−6701.

(15) Mao, X.; Song, X.; Lu, G.; Sun, Y.; Xu, Y.; Yu, J. Control of crystal morphology and size of calcium sulfate whiskers in aqueous HCl solutions by additives: experimental and molecular dynamics simulation studies. *Ind. Eng. Chem. Res.* **2015**, *54*, 4781−4787.

(16) Jia, C.; Chen, Q.; Zhou, X.; Wang, H.; Jiang, G.; Guan, B. Trace NaCl and Na₂EDTA mediated synthesis of alpha-calcium sulfate hemihydrate in glycerol-water solution. *Ind. Eng. Chem. Res.* **2016**, *55*, 9189−9194.

(17) Mao, X.; Song, X.; Lu, G.; Sun, Y.; Xu, Y.; Yu, J. Effects of metal ions on crystal morphology and size of calcium sulfate whiskers in aqueous HCl solutions. *Ind. Eng. Chem. Res.* **2014**, *53*, 17625−17635.

(18) Miao, M.; Feng, X.; Wang, G.; Cao, S.; Shi, W.; Shi, L. Direct transformation of FGD gypsum to calcium sulfate hemihydrate whiskers: Preparation, simulations, and process analysis. *Particuology* **2015**, *19*, 53−59.

(19) Fu, H.; Jia, C.; Chen, Q.; Jiang, G. Calcium sulfate polymorph evolution dominated by competitive nucleation in gypsum metastable zone. *J. Cryst. Growth* **2017**, *470*, 143−148.

(20) Tritschler, U.; Van Driessche, A. E. S.; Kempter, A.; Kellermeier, M.; Cölfen, H. Controlling the selective formation of calcium sulfate polymorphs at room temperature. *Angew. Chem., Int. Ed.* **2015**, *54*, 4083−4086.

(21) Reigl, S.; Van Driessche, A. E. S.; Mehringer, J.; Koltzenburg, S.; Kunz, W.; Kellermeier, M. Revisiting the roles of salinity, temperature and water activity in phase selection during calcium sulfate precipitation. *CrystEngComm* **2022**, *24*, 1529−1536.

(22) Singh, N. B.; Middendorf, B. Calcium sulphate hemihydrate hydration leading to gypsum crystallization. *Prog. Cryst. Growth Charact. Mater.* **2007**, *53*, 57−77.

(23) Freyer, D.; Voigt, W. Crystallization and phase stability of $CaSO_4$ and $CaSO_4$ based salts. *Monatsh. Chem.* **2003**, *134*, 693−719.

(24) Van Driessche, A. E. S.; Benning, L. G.; Rodriguez-Blanco, J. D.; Ossorio, M.; Bots, P.; García-Ruiz, J. M. The role and implications of bassanite as a stable precursor phase to gypsum precipitation. *Science* **2012**, *336*, 69−72.

(25) Stawski, T. M.; van Driessche, A. E. S.; Ossorio, M.; Rodriguez-Blanco, J. D.; Besselink, R.; Benning, L. G. Formation of calcium sulfate through the aggregation of sub-3 nanometre primary species. *Nat. Commun.* **2016**, *7*, 11177.

(26) Jiang, G.; Fu, H.; Savino, K.; Qian, J.; Wu, Z.; Guan, B. Nonlattice cation-SO_4^{2-} ion pairs in calcium sulfate hemihydrate nucleation. *Cryst. Growth Des.* **2013**, *13*, 5128−5134.

(27) Guan, Q.-J.; Sun, W.; Hu, Y.-H.; Yin, Z.-G.; Guan, C.-P. Synthesis of alpha-$CaSO_4 \cdot 0.5H_2O$ from flue gas desulfurization gypsum regulated by $C_4H_4O_4Na_2 \cdot 6H_2O$ and NaCl in glycerol-water solution. *RSC Adv.* **2017**, *7*, 27807−27815.

(28) Fu, H.; Jia, C.; Chen, Q.; Cao, X.; Zhang, X. Effect of particle size on the transformation kinetics of flue gas desulfurization gypsum to α-calcium sulfate hemihydrate under hydrothermal conditions. *Particuology* **2018**, *40*, 98−104.

(29) Dumazer, G.; Narayan, V.; Smith, A.; Lemarchand, A. Modeling gypsum crystallization on a submicrometric scale. *J. Phys. Chem. C* **2009**, *113*, 1189−1195.

(30) Rabizadeh, T.; Stawski, T. M.; Morgan, D. J.; Peacock, C. L.; Benning, L. G. The effects of inorganic additives on the nucleation and growth kinetics of calcium sulfate dihydrate crystals. *Cryst. Growth Des.* **2017**, *17*, 582−589.

(31) Ossorio, M.; Stawski, T.; Rodríguez-Blanco, J.; Sleutel, M.; García-Ruiz, J.; Benning, L.; Van Driessche, A. Physicochemical and additive controls on the multistep precipitation pathway of gypsum. *Minerals* **2017**, *7*, 140.

(32) Tang, Y.; Gao, J. Investigation of the Effects of Sodium Dicarboxylates on the Crystal Habit of Calcium Sulfate α-Hemihydrate. *Langmuir* **2017**, *33*, 9637−9644.

(33) Linnikov, O. D. Mechanism of aggregation and intergrowth of crystals during bulk crystallization from solutions. *Cryst. Res. Technol.* **2008**, *43*, 1268−1277.

(34) Wang, X.; Jin, B.; Yang, L.; Zhu, X. Effect of $CuCl_2$ on hydrothermal crystallization of calcium sulfate whiskers prepared from FGD gypsum. *Cryst. Res. Technol.* **2015**, *50*, 633−640.

(35) Chen, H.; Wang, J.; Hou, S.; Xiang, L. Influence of NH_4Cl on hydrothermal formation of alpha-$CaSO_4 \cdot 0.5H_2O$ whiskers. *J. Nanomater.* **2015**, *2015*, 670872.

(36) Fu, H.; Huang, J.; Shen, L.; Yu, Z.; Xu, L.; Li, J.; Cao, S.; Zhang, M.; Jiang, G. Role and fate of the lead during the conversion of calcium sulfate dihydrate to α-hemihydrate whiskers in ethylene glycol-water solutions. *Chem. Eng. J.* **2019**, *372*, 74−81.

(37) Fu, H.; Jiang, G.; Wang, H.; Wu, Z.; Guan, B. Solution-mediated transformation kinetics of calcium sulfate dihydrate to α-calcium sulfate hemihydrate in $CaCl_2$ solutions at elevated temperature. *Ind. Eng. Chem. Res.* **2013**, *52*, 17134−17139.

(38) Lagergren, S. K. About the theory of so-called adsorption of soluble substances. *Sven. Vetenskapsakad. Handingarl* **1898**, *24*, 1−39.

(39) Ho, Y. S.; McKay, G. Pseudo-second order model for sorption processes. *Process Biochem.* **1999**, *34*, 451−465.

(40) Lin, L.; Lei, Z.; Wang, L.; Liu, X.; Zhang, Y.; Wan, C.; Lee, D.-J.; Tay, J. H. Adsorption mechanisms of high-levels of ammonium onto natural and NaCl-modified zeolites. *Sep. Purif. Technol.* **2013**, *103*, 15−20.

(41) Moussavi, G.; Talebi, S.; Farrokhi, M.; Sabouti, R. M. The investigation of mechanism, kinetic and isotherm of ammonia and humic acid co-adsorption onto natural zeolite. *Chem. Eng. J.* **2011**, *171*, 1159−1169.

(42) Freundlich, H. Over the adsorption in solution. *J. Phys. Chem.* **1906**, *57*, 385−471.

(43) Langmuir, I. The constitution and fundamental properties of solids and liquids. Part I. solids. *J. Am. Chem. Soc.* **1916**, *38*, 2221−2295.

(44) Wang, X.; Wang, L.; Wang, Y.; Tan, R.; Ke, X.; Zhou, X.; Geng, J.; Hou, H.; Zhou, M. Calcium sulfate hemihydrate whiskers obtained from flue gas desulfurization gypsum and used for the adsorption removal of lead. *Crystals* **2017**, *7*, 270.